1

Graphene-Based Materials: Structure and Properties

Xiaoyang Deng[1,2] *and Yue Li*[1]

[1] *Tianjin University, School of Materials Science and Engineering and Tianjin Key Laboratory of Composites and Functional Materials, 135 Yaguan Rd., Jinnan District, Tianjin 300350, P.R. China*
[2] *Taiyuan University of Technology, Institute of New Carbon Materials, School of Materials Science and Engineering, P.R. China*

1.1 Introduction to Carbon Materials

Carbon materials have played important role in human society due to their extremely widespread applications, as shown in Figure 1.1. For example, while carbon black was used as paint, charcoal was as a heat source according to historical materials as early as the legend of Yao and Shun. Graphite is one of the most important carbon materials with numerous functions, including as electrodes in casting/stamping/pyrometallurgy processes, in powder form as pencil lead and polishing powder, as high-quality blocks in nuclear reactors, and as refractory materials for crucibles and molds. Diamond is the hardest three-dimensional carbon material. The rare, natural form of diamond is usually used in jewelry, while the synthetic form is used in cutting tools, infrared window materials, and abradants. In addition, carbon black is an important reinforcement material for tires in the development of automobiles. Conductive carbon black is important as a conductive additive in electrode production. Carbon fibers have been a star material in their use as additive-reinforcement materials in recent decades. For example, carbon-fiber-reinforced composite materials are widely used in aircraft body parts and aerospace field. In automobiles, carbon-fiber-reinforced carbon materials can be used in brakes production, while the motor-body manufacture is a promising application for carbon-fiber-based materials. In other fields, carbon-fiber-reinforced materials can be used to fabricate fan blades for wind power generation and in sports equipment. Some examples of applications of carbon materials are illustrated, but listing every application is not possible here due to the innumerable fields where they are used.

With the present rapidly rising world population and industrialization, energy demand has led to rigorous energy-sources consumption and environmental

Templated Fabrication of Graphene-Based Materials for Energy Applications, First Edition.
Edited by Chunnian He, Naiqin Zhao, and Junwei Sha.

Figure 1.1 Typical carbon materials, such as charcoals, pencil lead, diamond, and carbon black–reinforced tires. Source: Pixabay.com. Reproduced with permission of Pixabay.

pollution problem. Hence, the development of sustainable and clean energy technologies is a great challenge for human society, and the promising solutions are exploring solar/wind/tidal energies. Although these energy sources are renewable and clean, the highly intermittent feature makes them necessarily be coupled with the energy storage systems. On the other hand, the coming electronic and information age also requires high-performance energy storage equipment. Lithium-ion batteries and supercapacitors are the most widely used energy storage devices in industry and daily life – to name a few, electric vehicles, portable electronic equipment, and power station. Active carbon and graphite are used as active materials in the electrodes of supercapacitors and lithium-ion batteries, respectively; conductive carbon black is a commonly used additive to enhance the electrical conductivity of electrodes, while now carbon nanotube (CNT) and graphene are also used as conductive additives in some products.

Carbon materials are predominantly composed of carbon atoms, and they have diverse structures and properties. There are various methods for the classification of carbon materials according to different bases – e.g. the chemical bonding modes of the carbon–carbon atoms, the production process, micro/nano-texture, and time of appearance. According to the chemical feature of carbon–carbon bonding (Figure 1.2), various families of carbon materials have been defined: C—C bonds based on the sp^3 orbitals for the diamond family materials, C—C bonds based on sp^2 orbitals to construct graphite family, C—C bonds based on sp. orbitals for carbynes, and C—C bonds with hybrid orbitals, such as graphdiyne constructed by

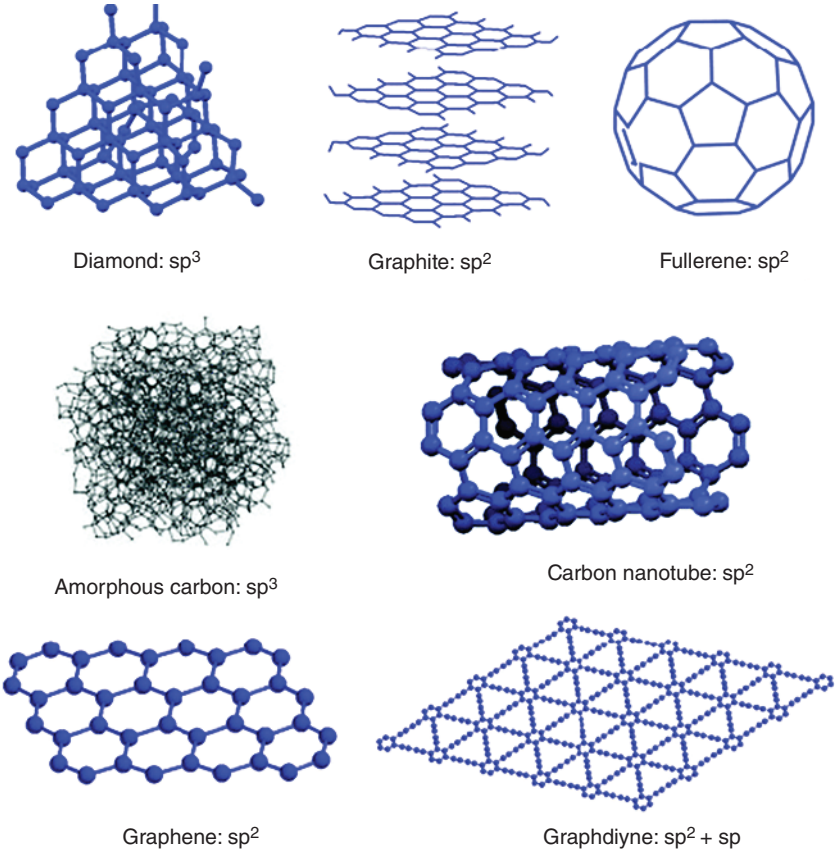

Figure 1.2 Carbon family based on carbon–carbon bonding. Source: Li et al. [1]. Reproduced with permission of Royal Society of Chemistry.

C—C bonds based on sp/sp^2 hybrid orbitals [2–5]. The most commonly used carbon materials in industry belong to the graphite family with a layered stack of carbon hexagons. Such carbon layers have strong anisotropy due to the strong covalent bonding based on sp^2 orbitals in the layers and weak bonding of van der Waals force of π electron clouds between stacked layers [4].

In the nanometer era, there have been many new members in the carbon family since the discovery of carbon nanomaterials. In 1985, zero-dimensional (0D) fullerene (C60) was first discovered with zero dimension by Smalley and coworkers [6, 7]. In 1991, the CNTs, a new one-dimensional (1D) carbon allotrope, were proposed by Iijima [8, 9]. The CNTs with various structures, i.e. thickness (single-, double-, or multi-walled), diameter, and length, have been synthesized and some types are produced on industrial scale [10]. When scaling down the thickness of graphite into nanoscale, graphene can be obtained; in other words, the monolayer graphene is the mono-unit of graphite. In 2004, graphene with two-dimensional (2D) structure was first experimentally evidenced and characterized by Geim and Novoselov, and it quickly became the most widely investigated material [11].

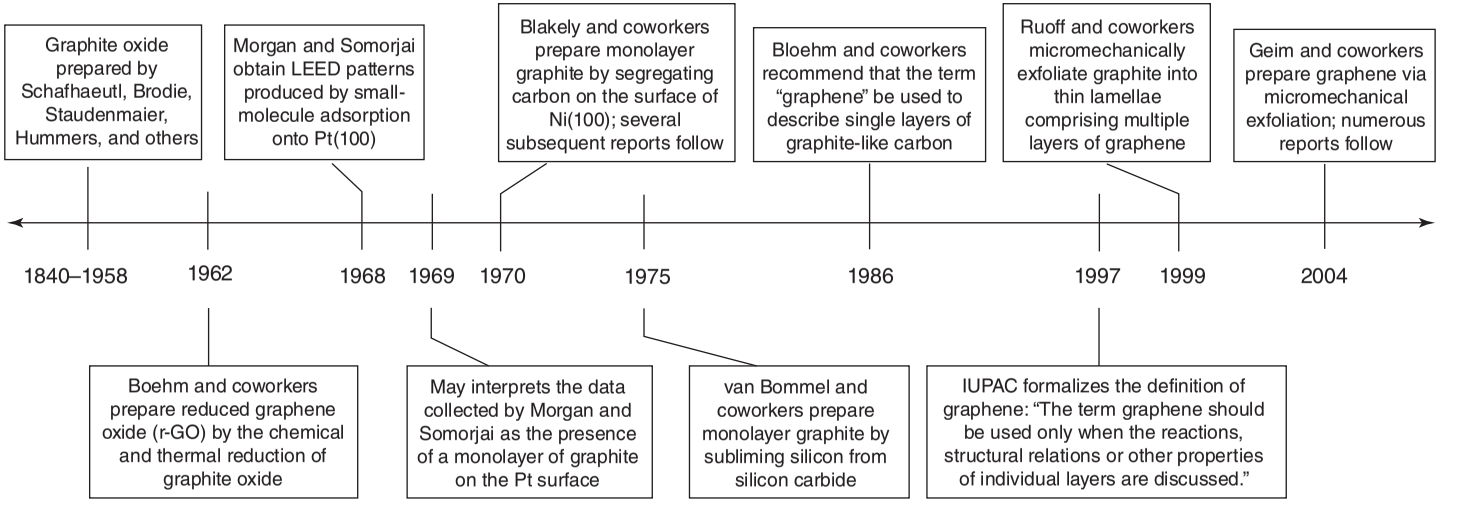

Figure 1.3 Timeline of selected events in the history of the preparation, isolation, and characterization of graphene. Source: Dreyer et al. [14]. Reproduced with permission of John Wiley and Sons.

1.2 History of Graphene

Despite a series of theoretical studies stating otherwise, as early as the 1940s, Wallace had advised that graphite might possess extraordinary electronic characteristics if its layer is isolated [12]. The term "graphene" was first proposed by Boehm et al. in 1986, who recommended that the term "graphene layer" should be used for the isolated graphitic structure constructed by only carbon atoms in one plane, which means that graphene is the most basic structure of graphite [13]. Geim, Novoselov, and coworkers used the mechanical approach to synthesize graphene in 2004, in which the highly ordered pyrolytic graphite surface was pressed against a surface of silicon wafer, and, when removed with a scotch tape, thin flakes of graphene were detected and characterized [11] (Figure 1.3). This was the first time that the existence of graphene was demonstrated through experimental evidence. In 2010, Geim and Novoselov were awarded a Nobel Prize for "groundbreaking experiments regarding the two-dimensional material graphene."

"Graphene," therefore, is defined as "an isolated single layer of carbon hexagons with sp^2-hybridized C—C bonding." In other words, as a new two-dimensional (2D) allotrope of carbon materials graphene has monoatomic thick honeycomb lattice structure (Figure 1.4a) [2, 15–18]. Hence, it can be considered as the basic building block to construct other graphitic materials, e.g. wrapped up into 0D fullerenes, rolled into 1D CNTs, and stacked to 3D graphite (Figure 1.4b) [15]. The distinctive structure and physical properties of graphene make it important for applications in technological field, such as polymer-based nanocomposites, energy storage and conversion devices (e.g. lithium-ion batteries, supercapacitors, air batteries, and fuel cells), flexible electronic and optical devices, and chemical sensors [2, 3, 19–22].

In general, some physical and chemical methods can be used to synthesize graphene, e.g. mechanical exfoliation of graphene layers from pristine graphite; chemical vapor deposition (CVD) of graphene layers on different crystals; thermal decomposition of silicon carbide (SiC); lengthwise unzipping of CNTs; exfoliation

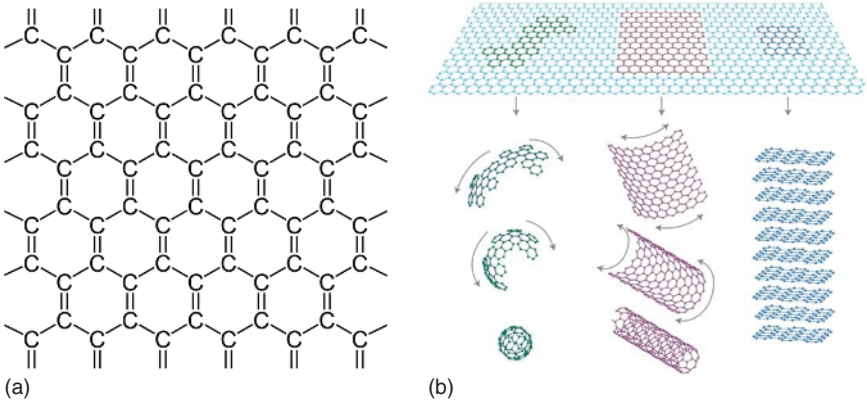

Figure 1.4 (a) Graphene structure and (b) mother of all graphitic forms. Source: Geim and Novoselov [15]. Reproduced with permission of Springer Nature.

of graphite through its intercalation compound; reduction of graphene oxides (GOs) and graphene fluoride; and organic synthesis processes [2, 23, 24]. But some methods, such as mechanical exfoliation, synthesis on SiC, and organic synthesis, exhibit difficulty in scalability and are expensive to produce, which restrict the widespread use of graphene. CVD method is unsuitable for large-scale production due to the high cost and rather low yield. The liquid-phase exfoliation process is so highly scalable and low cost that it can produce graphene in large quantities. Furthermore, although the reduced graphene oxide possesses low quality, it is still suitable for mass production due to the high yield and low cost.

1.3 Structure of Graphene

As shown in Figure 1.5a, the honeycomb lattice of graphene consists of two interpenetrating triangular sublattices, which are designated A and B. The sites of one sublattice (A) are at the centers of triangles (B) with a carbon-to-carbon interatomic length of 1.42 Å. Figure 1.5b shows the first Brillouin zone of graphene containing the high-symmetry points M, K, and K′. Each carbon atom has one *s* orbital and three p orbitals. The single s orbital is tied up with two in-plane p orbitals in the strong covalent bonding of graphene, which do not contribute to the conductivity. The remaining p orbital is oriented perpendicular to the molecular plane. This odd p orbital is hybridized to form π (valence) and π* (conduction) bands [27]. The π and π* bands touch at the K and K′ points (called Dirac points). The linear bands derived from crystal symmetry of graphene are a hallmark of graphene. This feature leads to many interesting physical properties, such as Berry's phase, half-integer quantum Hall effect (QHE), and Klein paradox. The energies of

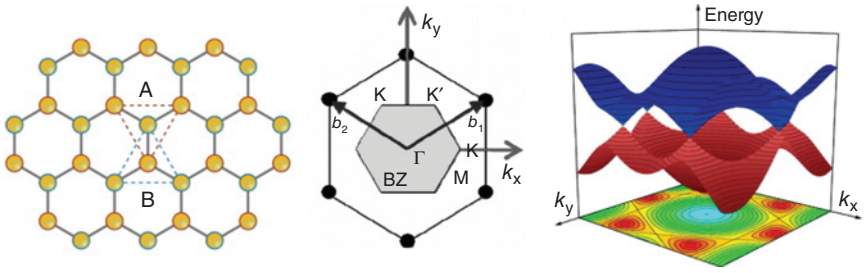

Figure 1.5 Atomic and electronic structures of graphene. (a) Graphene lattice consists of two interpenetrating triangular sublattices, each with different colors. The atoms at the sites of one sub-lattice, (i.e. A) are at the centers of the triangles defined by the other lattice (i.e. B), with a carbon-to-carbon interatomic length of 1.42 Å. Source: Rao et al. [25]. Reproduced with permission of John Wiley and Sons. (b) Reciprocal lattice of graphene. The shaded hexagon is the first Brillouin zone. (c) $\pi-\pi^*$ band structure of graphene. The three-dimensional first Brillouin zone is displayed in red and blue for the valence and conduction p bands, respectively, above the planar projection of the valence band. The six Dirac cones are positioned on a hexagonal lattice. Source: Soldano et al. [26]. Reproduced with permission of Elsevier).

the bands lie on the momentum of the charge carriers within the Brillouin zone. The constant energy contours within the linear-band approximation are circles around the K and K′ points [26]. As displayed in Figure 1.5c, the two bands meet each other and then produce cone-shaped valleys in the low-energy regime of the vicinity of the K and K′ points. In this low-energy limit, the dispersion relation of energy–momentum is linear and the carriers are seen as zero-rest mass relativistic particles. In the high-energy limit, the energy–momentum relation is changed and the distorted bands lead to anisotropy, also known as trigonal warping [26]. In addition, with stacked layers on top of each other, the electronic dispersion of graphene is changed. For example, the first-obtained bilayer graphene exhibits its own specific properties [25].

1.4 Properties of Graphene

Intrinsic (undoped) graphene is a semimetal or a semiconductor with zero bandgap. Pristine graphene possesses amazing properties, such as exceedingly high charge carriers (electrons and holes) mobility = 230 000 $cm^2\ V^{-1}\ s^{-1}$ at room temperature and an intriguing thermal conductivity of 4.84×10^3 to $5.30 \times 10^3\ W\ m^{-1}\ K^{-1}$ at room temperature [28]. Furthermore, graphene exhibits many mechanical properties, e.g. the high mechanical stiffness of about 1 TPa [29]. In addition, graphene has an ultrahigh surface area of about 2630 $m^2\ g^{-1}$, which is significantly higher than the CNT and graphite counterparts. Besides these, we will now give a detailed account of some properties of graphene.

The existence of massless Dirac quasiparticles in graphene may be verified through the experimental observation, based on the code that the cyclotron mass was dependent on the square root of the electronic density in graphene [30, 31]. Graphene can exhibit an ambipolar electric field effect due to the zero bandgap semiconductor feature. The charge carriers in graphene can be tuned continuously between electrons and holes with concentrations as high as 1013 cm^{-2}, and mobilities of up to 15 000 $cm^2\ V^{-1}\ s^{-1}$ even under ambient conditions (Figure 1.6) [15, 30, 31]. Moreover, the low dependence of mobilities of charge carriers in graphene with temperature suggests that ultrahigh mobility would be accomplished at room temperature [32]. More importantly, when minimizing the influence of impurity scattering, mobilities in excess of 200 000 $cm^2\ V^{-1}\ s^{-1}$ could be achieved in suspended graphene [33]. The mobilities in graphene can still remain high even at a huge carrier concentration (>1012 cm^{-2}) in both electrically and chemically doped devices [34, 35]. Another measure of the electronic quality of graphene is that the QHE can be directly observed even at room temperature, which increases the temperature range for the QHE by a factor of 10 compared with previous reports [36].

Based on the Wiedemann–Franz law, the contribution of electronics is negligible for thermal conductivity in graphene; hence, the thermal conductivity (κ) of graphene is just dependent on phonon transport, namely high-temperature diffusive conduction and low-temperature ballistic conduction [37]. As early as

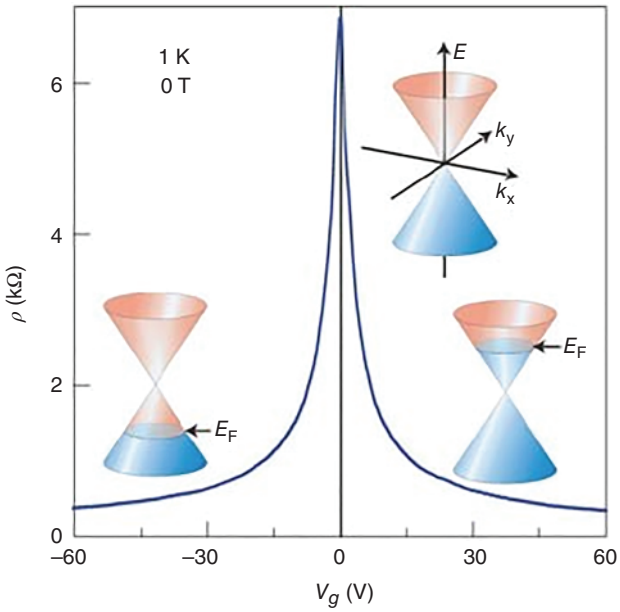

Figure 1.6 Ambipolar electric field effect in single-layer graphene. The rapid decrease in resistivity ρ on adding charge carriers indicates their high mobility (in this case, $\mu \approx 5000\,\mathrm{cm^2\,V^{-1}\,s^{-1}}$ and does not noticeably change with increasing temperature to 300 K). Source: Geim and Novoselov [15]. Reproduced with permission of Springer Nature.

2000, the thermal conductivity of suspended monolayer graphene was predicted to be about $6000\,\mathrm{W\,m^{-1}\,K^{-1}}$ at room temperature, much higher than that of graphitic carbon [38]. For a suspended monolayer graphene flake obtained from mechanical exfoliation, a high thermal conductivity value of about $5000\,\mathrm{W\,m^{-1}\,K^{-1}}$ was observed through an optical measurement according to the shift of Raman G band [28].

The mechanical properties, including Young's modulus and fracture strength of monolayer graphene, have been investigated by atomic force microscopy (AFM) and numerical simulations (e.g. molecular dynamics) [39]. Particularly, the nanoindentation technique was measured using AFM to detect elastic properties and intrinsic breaking strength for free-standing monolayer graphene [29]. The results displayed that Young's modulus and fracture strength of defect-free graphene can reach 1.0 TPa and 130 GPa, respectively. The mechanical properties of some graphene materials, produced by reducing the graphene oxide, were investigated but exhibited decreased properties compared with the defect-free monolayer graphene [40–42].

The measured white light absorbances of one- and two-layered suspended graphene sheets are 2.3% and 4.6%, respectively. According to the experimental observation, the transmittance was linearly decreased based on the number of layers for *n*-layer graphene, and the strict linearity feature has been further demonstrated up to five monolayers [43]. This macroscopic linear dependence between the transmittance and the thickness of graphene films is intimately related to the

two-dimensional gapless electronic structure of graphene. However, when the energy of incident photons was lower than 0.5 eV, a deviation from the universal linear behavior could be observed. This deviation can be attributed to the finite temperature and chemical potential shift of the charge-neutrality (Dirac) point induced by doping [44].

1.5 Structure Defects of Graphene

To adapt to different application fields, one of the research focuses on graphene is the targeted control of its key physical and chemical properties. For this purpose, various modification methods are developed. Among them, defect engineering is considered an efficient method that can tailor mechanical, electrical, chemical, and magnetic properties of graphene [45–47]. Structural defects of graphene can be divided into two main categories. The first type is **intrinsic defects**, composed of non-sp^2 orbit hybrid carbon atoms on graphene. The carbon atomic orbital hybrid forms of change are usually caused by the absence of extra carbon atoms in the surrounding carbon six-membered rings. Therefore, obvious holes in non-six-membered carbon rings or even point or line domains can be observed in this graphene sheet at atomic resolution. The second type is **extrinsic defects**, which are generated by foreign (non-carbon) atoms covalently bonded to graphene carbon atoms. The foreign atoms (such as N, O, and B) strongly affect the charge distribution and properties of graphene [48, 49].

Specifically, **graphene intrinsic defects** can be divided into five categories: Stone–Wales defects, linear defects, single vacancies, multiple vacancies, and carbon adatoms defects. **Stone–Wales defect** is caused by simply rotating the C—C bonds to form different carbon polygon combinations (switching between pentagons, hexagons, and heptagons) without adding or removing carbon atoms. Figure 1.7 demonstrates typical Stone–Wales defects formed by rotating a C—C bond by 90° (within four neighboring hexagons that transform to two pentagons and two heptagons: $C_{6,6,6,6} \rightarrow C_{5,5} + C_{7,7}$) [50, 51]. Continuous rotation of C—C bond can be extended to linear defects consisting of paired pentagons and heptagons, as shown in Figure 1.7c. Such defects also require relatively large energy to form (~5 eV), so they can be produced by electron-beam bombardment or rapid cooling at high temperatures [52]. The existence of Stone–Wales defects significantly affects the electrical conductivity of graphene and enhances its electrochemical activity, but its strength decreases significantly [53].

Single vacancies can be considered as the simplest defects, which are formed by a missing carbon atom from continuous planar carbon six-membered ring. Similarly, on the basis of single vacancies, a continued absence of carbon atoms leads to **multiple vacancies**. Figure 1.8 displays the TEM photographs and typical atomic structures of single vacancies and multiple vacancies. The absence of dangling bonds and the steady rotation of C—C bonds make the $V_{2(555\text{-}777)}$ (7 eV) have lower formation energy than $V_{1(5\text{-}9)}$ (7.5 eV) and $V_{2(5\text{-}8\text{-}5)}$ (8 eV), so the probability of the $V_{2(555\text{-}777)}$ defect being observed by TEM is indeed greater [55, 56].

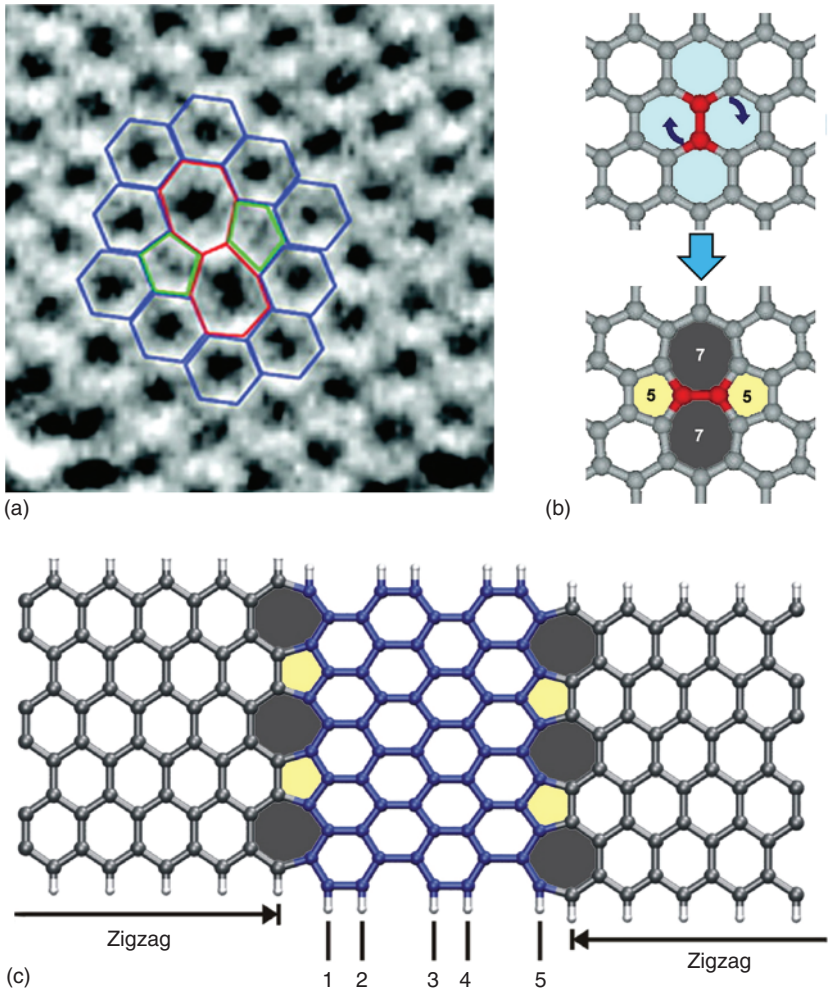

Figure 1.7 TEM image. (Source: Meyer et al. [50]. Reproduced with permission of American Chemical Society) (a) and (b) atomic structure of Stone–Wales defect in graphene by rotating a C—C bond by 90°. Source: Terrones et al. [51] Reproduced with permission of Elsevier. (c) Atomic structure of linear defect with a chain of paired rings (pentagons and heptagons). Source: Terrones et al. [51] Reproduced with permission of Elsevier.

1.5.1 Carbon Adatoms Defects

Free carbon atoms interacting with the desirable planar graphene region may destroy the original planar structure of graphene and cause sp^3-hybridization defects [57]. Figure 1.9 exhibits the spatial arrangement of carbon adatoms defects and introduction positions of free carbon atoms. The existence of carbon adatoms defects undoubtedly destroys the two-dimensional crystal structure of graphene. In particular, some defects (as presented in Figure 1.9b) directly change the orbital sp^2-hybridization type to sp^3-hybridization, which are bound to affect the electrical properties of graphene. Indeed, making such defects manageable is a big challenge for researchers.

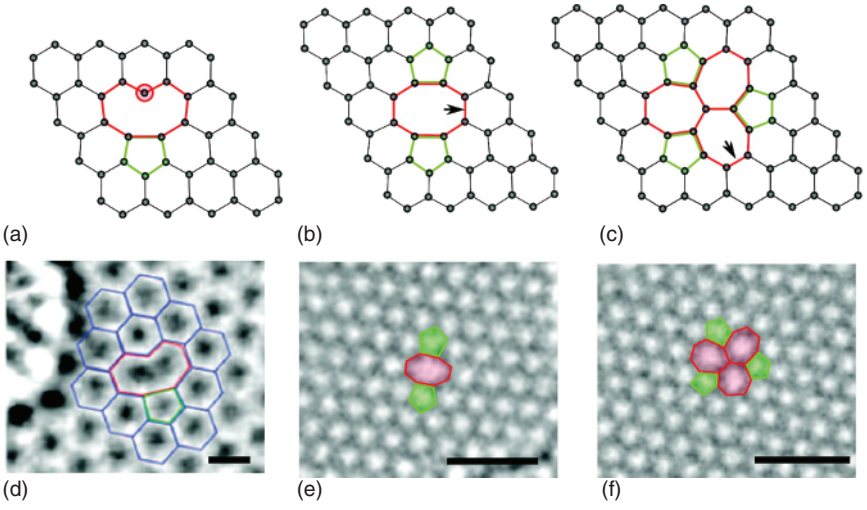

Figure 1.8 Atomic structures and TEM images of single-vacancy $V_{1(5\text{-}9)}$ (a, d), double-vacancy $V_{2(5\text{-}8\text{-}5)}$ (b, e), and $V_{2(555\text{-}777)}$ (c, f) defects in graphene. Source: Banhart et al. [54]. Reproduced with permission of American Chemical Society).

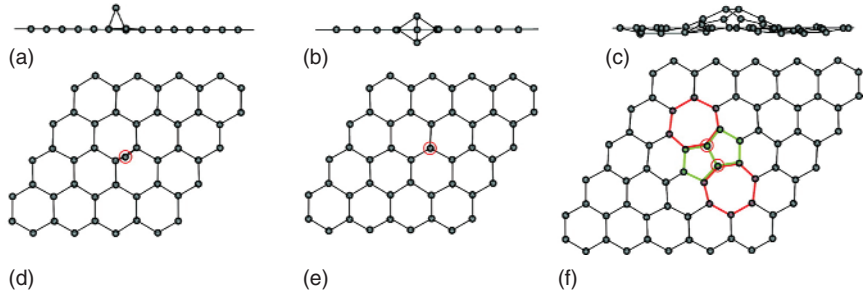

Figure 1.9 Atomic structures of carbon adatoms: (a, d) single adatom in the bridge; (b, e) single adatom in the dumbbell configuration; (c, f) the C_{7557} defect formed by two close adatoms. Source: Banhart et al. [54]. Reproduced with permission of American Chemical Society.

1.5.2 Graphene Extrinsic Defects

Graphene extrinsic defects can be classified as out-of-plane and in-plane heteroatom-introduced defects according to the position of introduction. Under the conditions of CVD or strong oxidation, metal atoms or oxygen-containing functional groups are inevitably introduced on the surface of graphene, resulting in **out-of-plane heteroatom-introduced defects**. Figure 1.10 demonstrates the structure diagram of graphene with out-of-plane defects introduced by metal and oxygen adatoms. The metal adatom can cause obvious migration movement on the graphene layer, and the different metal adatoms can effectively regulate the electronic and magnetic properties of graphene sheets [57, 59]. The graphene-containing oxygen functional group prepared by strong oxidant has obvious better hydrophilicity than graphene. Based on the particularity of this

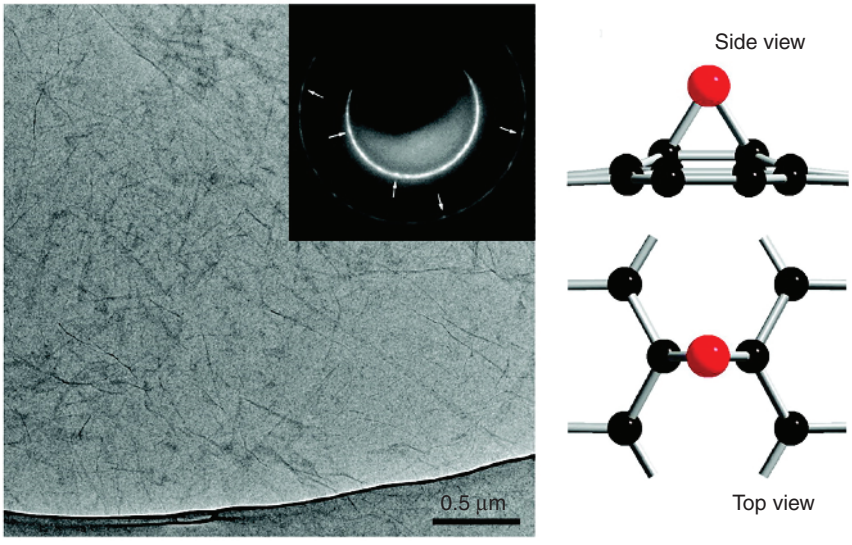

Figure 1.10 TEM image and corresponding atomic structure of GO films. The inset is the diffraction pattern from these GO films. Source: Mkhoyan et al. [58]. Reproduced with permission of American Chemical Society.

material and its broad application prospect, this material is named as graphene oxide (GO). Actually, the oxygen adatoms are difficult to be completely removed in the subsequent reduction process, and the relative content of graphene defects does not change or even increase, which is because when oxygen atoms are removed, carbon atoms are removed at the same time to form cavities, inducing intrinsic defects [58]. **In-plane introduced defects**: Doping by foreign atoms, such as nitrogen and boron, can form three chemical bonds and thus can replace the carbon atoms in graphene, which constitute the **in-plane introduced defects** in graphene. B and N doping affect the charge distribution on the carbon atoms in the sublattice of the substituted dopant. As foreign atoms, N and B atoms also have their own unique properties, which also change the properties of graphene. Moreover, the B- and N-doped graphene exhibit higher electrical conductivity than the pristine graphene [48]. Therefore, researchers are committed to developing and studying heteroatom-doped graphene with excellent catalytic activity and electrical conductivity [60–62].

1.6 Different Dimensional Graphene

According to the different dimensions of graphene nanostructures discovered, graphene can be divided into **0-dimensional (0D) graphene clusters, one-dimensional (1D) graphene nanoribbons, two-dimensional (2D) graphene sheets, and three-dimensional (3D) graphene architectures.** The lateral dimensions of graphene materials vary from nanoscale to microscale to

macroscopic, which may affect permeability thresholds, bandgaps, and many other properties and behaviors. When lateral dimensions of graphene materials are extremely limited into nanoscale, three incongruous atoms in the edges would be formed. As this chain-like structure exhibits a cyclic sequence with a larger aspect ratio, 1D sp^2 hybridized carbon crystal graphene nanoribbon was formed. However, if the chains present dimensionless sexual or no periodicity, this structure can be seen as a 0D graphene cluster [51]. Graphene clusters have a large number of dangling bonds of edge atoms, so the structure is quite unstable. The diversity of possible types of graphene clusters significantly hinders the theoretical exploration of the regularities of changes in their properties that vary with many factors (such as size, shape, temperature, and charge). According to this situation, few types of graphene clusters were simulated [63, 64].

Graphene nanoribbons usually exhibit two different possible edge geometries, so-called zigzag and armchair, as shown in Figure 1.11a, which exhibit very different electronic properties due to their contrasting boundary conditions. Early tight-binding calculations suggested that the structure of narrow bands depended on their orientation. These results show the zigzag graphene nanoribbons (ZGNRs) are always metallic (top of Figure 1.11b), and the armchair graphene nanoribbons (AGNRs) show alternate metal structure and gap electronic structure according to the width (bottom of Figure 1.11b). However, for ZGNRs, first-principle calculations verify that the flat band of the high density-of-states (DOS) at zero energy calculated by simple tight-binding calculations is unstable relative to spin splitting.

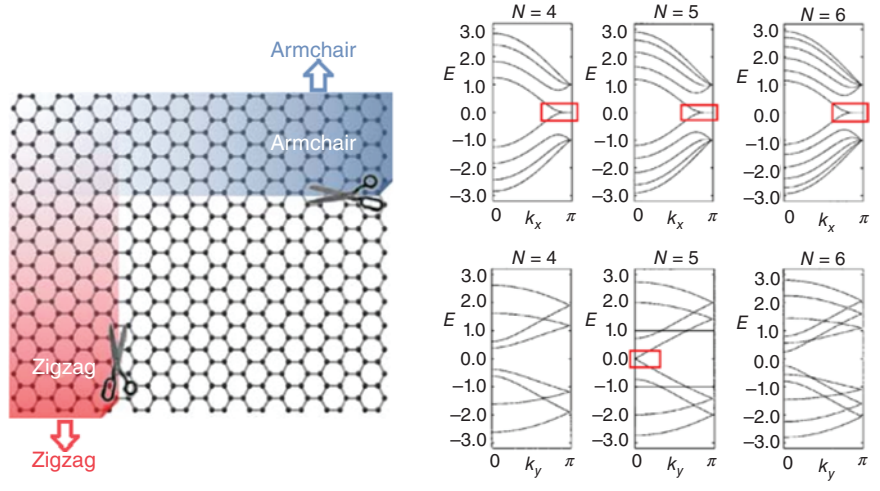

Figure 1.11 (a) The schematic representation of cutting the two-dimensional graphene sheet to obtain ZGNRs and AGNRs [65]. Source: Dutta and Pati [65]. Reproduced with permission of Royal Society of Chemistry. (b) Electronic band structure obtained by tight-binding calculations for various graphene nanoribbon widths. The width is measured by N carbon dimer lines ($N = 4, 5, 6$). Top row: ZGNRs have a metallic state at $E = 0$. Bottom row: AGNRs exhibit alternating metallic and semiconducting behaviors with changing value of N. Source: Nakada et al. [66]. Reproduced with permission of Royal Society of Chemistry.

Because the edge of the narrow ZGNRs is very close to charge neutral, electron conductance tends to be in a spin direction. Using the electric field in-plane to modify the natural energy distribution of spin in the band, semi-metallicity was proposed [67]. At present, the preparation methods of graphene nanoribbons mainly include lithographic-patterning methods (etching graphene) [68], chemical methods (cutting CNTs or other graphitic precursors) [68, 69], CVD methods [70, 71], and organic synthesis [72]. As a two-dimensional variant of graphene, GNRs have room-temperature QHE and higher electron migration. Due to their excellent performance, GNRs demonstrate more flexible and controllable performance than graphene and have a broader application prospect, which presents great development potential in the **fields of polymer modification, lithium-ion battery, fuel cell, and other energy storage materials** and electronic devices.

1.6.1 3D Graphene Architectures (3DG)

In practical applications, 2D graphene sheets are prone to stacking and agglomeration, which significantly reduces specific surface area and electrical conductivity compared with intrinsic graphene. 3D graphene architectures, as 3D derivatives of graphene, not only maintain good electronic conductivity, heat stability, oil-absorption, lightweight, and biocompatible properties inherited from graphene, but also process stable structure and high-surface utilization. Therefore, 3DG has great development prospects in the fields of electronic devices, environmental cleanup, shock damping, biomedical sciences, and nanocomposites.

As usual, 3DG with few defects can be directly prepared on a porous metal template (e.g. Ni, Cu foam). Qin et al. synthesized the 3D porous graphene (3DPG) by CVD method using porous Cu as template and catalysts [73]. The 3DPG exhibits large specific surface area ($1160\,m^2\ g^{-1}$) and desirable electrochemical performance. Furthermore, the obtained 3DPG can be used to make composite (e.g. $3DPG/MnO_2$) for electrochemical applications [74]. To obtain 3DG with a large number of defects and functional groups, the common strategies to achieve macroscopic preparation of 3DG are the facile and versatile graphene oxide (GO)-based chemical synthesis methods [75]. However, the GO is usually produced by using strong oxidizing reagents, which are not suitable for environmental considerations. As a consequence, environment-friendly, mass-produced, and cost-effective salt template methods based on soluble organic matter have become considerable strategies to synthesize 3DG [76]. The 3DG was formed by the space limitation of self-assembled salt template during the pyrolysis of organics [77]. By adjusting the type and combination of salt templates, 3DG with special porous structure can be designed to adapt to various electrochemical applications [78]. In addition, through the selection of appropriate organics, heteroatom-doped 3DG materials have been synthesized, endowing them special physical and chemical properties [79, 80].

In recent years, utilizing 3D printing technology to prepare 3DG has also received considerable attention from researchers. Ink-based 3D printed 3DG, GO, or chemically modified graphene is often used as precursors or as additives for printable

inks [81]. Jiang et al. reported a facile ion-induced gelation method to directly print 3D graphene aerogel microlattices (GAMs) from GO-based ink with trace additives [82]. Due to the rich porous structure and fast electronic transmission, 3D GAMs exhibited admirable electrochemical performances as electrode material for supercapacitors. Sha et al. used Ni powder and sucrose powder as precursors, commercial CO_2 lasers for 3D printing in atmosphere conditions at room temperature, and obtained 3D graphene foam (3DGF) with high porosity (~99.3%), low density (~0.015 g cm^{-3}), high quality, good damping performance (~0.06), and electrical conductivity (~8.7 S cm^{-1}) [83]. This strategy combines 3D printing technology and template powder metallurgy technology, and exhibits the characteristics of simplicity, efficiency, and strong designability.

1.7 Graphene Composites

To utilize its admirable properties, graphene was used as a typical modified phase to prepare functional graphene–based composites, which have shown excellent application potential in many technical fields, such as electronics, biomedicine, machinery, and aerospace. At present, the energy storage researches of functional graphene–based materials mainly focus on **graphene/conductive polymer composites** and **graphene/inorganic composites**.

1.7.1 Graphene/Conductive Polymer Composites

Conductive polymers, such as polyaniline (PANI), polyacrylonitrile (PAN), polypyrrole (PPy), poly(3,4-ethylenedioxythiophene) (PEDOT), are commonly used to prepare graphene/conductive polymer composites [84–86]. Conductive polymers have the advantages of high energy storage capacity, good electrical conductivity, and low cost. However, the poor mechanical strength performance restricts their electrochemical stability and further application [87]. Therefore, during preparation, graphene is not only required to maintain decentralized structure, but also for effective interface interaction with polymer to achieve the synergistic effect between polymer and graphene.

Up to now, the main methods of preparing graphene/conductive polymer nanocomposites include in situ polymerization, electronic deposition, and hydrothermal synthesis. Zhang et al. prepared 3D PPy-coated porous graphene (PPy/PG) composites by in situ polymerization [88]. The PPy/PG displays a 3D hierarchical porous structure, which can provide a conductive trap and a stable skeleton to lithium polysulfides, thereby improving the cycling performance. Hu et al. combined electrostatic self-assembly approach and hydrothermal reduction method for synthesizing continuous 3D rGO/PANI composite [89]. 3D rGO/PANI possesses interconnected 3D macroporous networks, and the PANI nanofibers are tightly wrapped inside graphene, which can improve the conductivity and the structural stability of PANI effectively. Moreover, self-assembled 3D rGO/PANI also shows good flexibility, which can be fabricated to a flexible storage device.

1.7.2 Graphene/Inorganic Composites

The insertion of inorganic materials can reduce the interaction between graphene sheets, while the combination of graphene with specific inorganic phase can avoid single material deficiencies and a wide application prospect in the field of energy storage [90, 91]. Inorganic materials, mainly including metal and metallic compounds, Si-based materials, and P-based materials, are widely studied materials compound with graphene [90, 92–94].

Chemical reduction is a common method of preparing metal/graphene composites by chemically reducing some metal precursors on the surface of graphene. Lv et al. utilized nano-zeolites as template, $Pt(NH_3)_4Cl_2$ as Pt sources, and developed a novel in situ confined growth route for constructing Pt nanoparticles@graphene nanobox composites [95]. Due to the good dispersion of ultrafine Pt nanoparticles in 3D hollow box graphene skeleton, Pt nanoparticles@graphene nanobox exhibited excellent electrocatalytic activity for the ORR. Qin et al. synthesized SnSb-in-plane nanoconfined 3D N-doped porous graphene network (3D SnSb@N-PG) by a simple spray drying followed by annealing strategy. The 3D continuously interconnected porous structure, derived from the NaCl template, provides 3D conductive network, and the reduced SnSb nanoparticles were tightly trapped by graphene nanosheets; such microstructure ensures good mechanical stability and electronic conductivity [80].

Hydrothermal synthesis is a simple method that can generate high pressure under high temperature and fixed volume to prepare graphene/inorganic composites, and it is also a high-efficiency and low-cost method for industry application. Perera et al. prepared TiO_2/graphene composite materials by an alkaline hydrothermal method and found that the average diameter of TiO_2 nanotubes was about 9 nm, which were evenly dispersed on the graphene nanosheets [96]. By using one-pot hydrothermal method, Ye et al. prepared graphene/metal sulfides ($SnCoS_4$, CoS_2, and SnS_2) composites. The cobalt sulfides nanoparticles nucleation and growth on graphene surface make the nanoparticles dispersion and size more uniform. The structure of $SnCoS_4$/graphene composites, the high intrinsic conductivity of graphene, and large specific surface area give it superior electrochemical properties when used as lithium-ion battery anode materials [97].

Electrodeposition of inorganic nanomaterials on graphene matrix is a green and efficient method for preparing graphene/inorganic composites. Kuang et al. prepared Ni/graphene composites by electrochemical deposition method and found that when the content of graphene was 0.2%, the thermal conductivity of the composites was 15% higher than that of pure Ni [98]. Gao et al. synthesized graphene-wrapped mesoporous $MnCO_3$ composite through dynamic floating electrodeposition method and achieved the reduction of GO, and deposition and embedding of $MnCO_3$ in one-step electrodeposition [99]. Li et al. deposited active amorphous manganese oxide (a-MnO_x) on the surface of 3D graphene–CNT composites, resulting in good conductivity and porosity for the high-performance storage application [100].

Sol–gel method is also commonly used to prepare graphene/inorganic composite materials, which mainly carries out a series of hydrolysis and condensation polymerization reactions of the metal alkoxide or metal chloride precursor. Giampiccolo et al. reported a TiO_2/graphene composite prepared by simple sol–gel method. They employed a promising catalyst for NO_2 sensor [101]. Similarly, Li et al. used tetrabutyl titanate (TBOT) as the Ti precursor, ammonia solution as hydrolysis accelerator, and GO sheets as substrate; and synthesized sandwiched TiO_2/graphene composite by sol–gel and annealing route [102]. Besides these, the sol–gel method usually can be used to prepare other graphene/inorganic composites, such as $Li_4Ti_5O_{12}$/graphene [103], SiO_2/graphene [104], and ZnO/graphene [105].

1.8 Applications of Graphene

Since the discovery and successful preparation, graphene with excellent physical and chemical properties, such as high Young's modulus (~1100 GPa), high conductivity (200 S m^{-1}), high coefficient of thermal conductivity (~5000 W m^{-1} K^{-1}), high specific surface area (2630 m^2 g^{-1}), high carrier mobility (200 000 cm^2 V^{-1} s^{-1}), and high light transmittance, has been thought to trigger the next industrial revolution [26, 28, 33]. In all applied fields, especially in new-energy vehicles, aerospace, intelligent electronic equipment, and other high-tech fields, graphene is considered a key material to break through existing technical barriers.

Chen et al. reported good electrochemical lithium storage properties (at current density of 0.1 C, 1 C = 744 mA g^{-1}) of graphene with high degree of crystallization [106]. Zhao et al. systematically studied the capacitance characteristics of rGO with a specific capacitance of 260.5 F g^{-1} [107]. Graphene also has unique advantages in solar cell applications. Graphene has good light transmittance and electrical conductivity, and is considered as a potential substitute material for expensive and poisonous indium tin oxide (ITO). Lewis et al. used graphene as the electrode and obtained highly efficient organic solar cells (1.18%), very close to that of ITO (1.21%) [108]. In recent years, with the realization of graphene-controllable preparation and the deepening of application research, the efficiency of graphene-based solar cells has been improved continuously. 3D graphene materials have been proved as a promising counter electrode for dye-sensitized solar cells, which showed a desirable PCE of 7.63% and the possibility of replacing Pt [109]. Hwang et al. prepared graphene-reinforced copper matrix composites by means of molecular mixing. Compared with pure Cu, the elastic modulus and yield strength of the composites were increased by 30% and 80%, as the addition of GO is 2.5 vol% [110]. Li et al. prepared Al/3D graphene foam composite by variable speed-ball milling and adding pore forming. The graphene-reinforced aluminum matrix composites exhibited intelligent compression performance and energy absorption capacity [111].

Although many companies and enterprises claim to have prepared the new generation of graphene batteries, cars, supercapacitors, and so on, most of them are more of a gimmick than reality. The age of graphene is approaching, but not yet. There is still a lot of work to be done in the research of graphene, which needs to be further studied in depth. It still needs the continuous efforts and exploration of the majority of scientific research workers to promote it from the laboratory to the industry and market and benefit human society.

References

1 Li, Y., Xu, L., Liu, H. et al. (2014). Graphdiyne and graphyne: from theoretical predictions to practical construction. *Chemical Society Reviews* 43 (8): 2572–2586.
2 Raccichini, R., Varzi, A., Passerini, S. et al. (2015). The role of graphene for electrochemical energy storage. *Nature Materials* 14 (3): 271–279.
3 Shehzad, K., Xu, Y., Gao, C. et al. (2016). Three-dimensional macro-structures of two-dimensional nanomaterials. *Chemical Society Reviews* 45 (20): 5541–5588.
4 Rajib, P., Feng, D., Liming, D. et al. (2019). 3D heteroatom-doped carbon nanomaterials as multifunctional metal-free catalysts for integrated energy devices. *Advanced Materials* 31: 1805598.
5 Li, G., Li, Y., Liu, H. et al. (2010). Architecture of graphdiyne nanoscale films. *Chemical Communication* 46 (19): 3256–3258.
6 Kroto, H.W., Heath, J.R., O'Brien, S.C. et al. (1985). C60: Buckminsterfullerene. *Nature* 318 (6042): 162–163.
7 Krätschmer, W., Lamb, L.D., Fostiropoulos, K. et al. (1990). Solid C60: a new form of carbon. *Nature* 347 (6291): 354–358.
8 Iijima, S. (1991). Helical microtubules of graphitic carbon. *Nature* 354 (6348): 56–58.
9 Iijima, S. and Ichihashi, T. (1993). Single-shell carbon nanotubes of 1-nm diameter. *Nature* 363 (6430): 603–605.
10 Chen, X., Paul, R., and Dai, L. (2017). Carbon-based supercapacitors for efficient energy storage. *National Science Review* 4 (3): 453–489.
11 Novoselov, K.S., Geim, A.K., Morozov, S.V. et al. (2004). Electric field effect in atomically thin carbon films. *Science* 306 (5696): 666–669.
12 Wallace, P.R. (1947). The band theory of graphite. *Physical Review* 71 (9): 622–634.
13 Boehm, H.P., Setton, R., and Stumpp, E. (1994). Nomenclature and terminology of graphite intercalation compounds. *Pure and Applied Chemistry. Chimie pure et appliqueé* 66 (9): 1893.
14 Dreyer, D.R., Ruoff, R.S., and Bielawski, C.W. (2010). From conception to realization: an historial account of graphene and some perspectives for its future. *Angewandte Chemie* 49 (49): 9336–9344.
15 Geim, A.K. and Novoselov, K.S. (2007). The rise of graphene. *Nature Materials* 6 (3): 183–191.

16 Bianco, A., Cheng, H.-M., Enoki, T. et al. (2013). All in the graphene family – a recommended nomenclature for two-dimensional carbon materials. *Carbon* 65: 1–6.

17 Chen, Z., Ren, W., Gao, L. et al. (2011). Three-dimensional flexible and conductive interconnected graphene networks grown by chemical vapour deposition. *Nature Materials* 10 (6): 424–428.

18 Li, X., Cai, W., An, J. et al. (2009). Large-area synthesis of high-quality and uniform graphene films on copper foils. *Science* 324 (5932): 1312–1314.

19 Wang, Z., Gao, H., Zhang, Q. et al. (2019). Recent advances in 3D graphene architectures and their composites for energy storage applications. *Small* 15 (3): e1803858.

20 Lv, W., Li, Z., Deng, Y. et al. (2016). Graphene-based materials for electrochemical energy storage devices: Opportunities and challenges. *Energy Storage Materials* 2: 107–138.

21 Randviir, E.P., Brownson, D.A.C., and Banks, C.E. (2014). A decade of graphene research: production, applications and outlook. *Materials Today* 17 (9): 426–432.

22 Ji, L., Meduri, P., Agubra, V. et al. (2016). Graphene-based nanocomposites for energy storage. *Advanced Energy Materials* 6 (16): 1502159.

23 Novoselov, K.S., Fal'ko, V.I., Colombo, L. et al. (2012). A roadmap for graphene. *Nature* 490 (7419): 192–200.

24 Han, S., Wu, D., Li, S. et al. (2014). Porous graphene materials for advanced electrochemical energy storage and conversion devices. *Advanced Materials* 26 (6): 849–864.

25 Rao, C.N., Sood, A.K., Subrahmanyam, K.S. et al. (2009). Graphene: the new two-dimensional nanomaterial. *Angewandte Chemie* 48 (42): 7752–7777.

26 Soldano, C., Mahmood, A., and Dujardin, E. (2010). Production, properties and potential of graphene. *Carbon* 48 (8): 2127–2150.

27 Geim, A.K. and MacDonald, A.H. (2007). Graphene: Exploring carbon flatland. *Physics Today* 60 (8): 35–41.

28 Balandin, A.A., Ghosh, S., Bao, W. et al. (2008). Superior thermal conductivity of single-layer graphene. *Nano Letters* 8 (3): 902–907.

29 Lee, C., Wei, X., Kysar, J.W. et al. (2008). Measurement of the elastic properties and intrinsic strength of monolayer graphene. *Science* 321 (5887): 385–388.

30 Zhang, Y., Tan, Y.W., Stormer, H.L. et al. (2005). Experimental observation of the quantum Hall effect and Berry's phase in graphene. *Nature* 438 (7065): 201–204.

31 Novoselov, K.S., Geim, A.K., Morozov, S.V. et al. (2005). Two-dimensional gas of massless Dirac fermions in graphene. *Nature* 438 (7065): 197–200.

32 Morozov, S.V., Novoselov, K.S., Katsnelson, M.I. et al. (2008). Giant intrinsic carrier mobilities in graphene and its bilayer. *Physical Review Letters* 100 (1): 016602.

33 Bolotin, K.I., Sikes, K.J., Jiang, Z. et al. (2008). Ultrahigh electron mobility in suspended graphene. *Solid State Communications* 146 (9–10): 351–355.

34 Schedin, F., Geim, A.K., Morozov, S.V. et al. (2007). Detection of individual gas molecules adsorbed on graphene. *Nature Materials* 6 (9): 652–655.

35 Du, X., Skachko, I., Barker, A. et al. (2008). Approaching ballistic transport in suspended graphene. *Nature Nanotechnology* 3 (8): 491–495.

36 Novoselov, K.S., Jiang, Z., Zhang, Y. et al. (2007). Room-temperature quantum Hall effect in graphene. *Science* 315 (5817): 1379.

37 Yu, C., Shi, L., Yao, Z. et al. (2005). Thermal conductance and thermopower of an individual single-wall carbon nanotube. *Nano Letters* 5 (9): 1842–1846.

38 Berber, S., Kwon, Y.K., and Tomanek, D. (2000). Unusually high thermal conductivity of carbon nanotubes. *Physical Review Letters* 84 (20): 4613–4616.

39 Zhu, Y., Murali, S., Cai, W. et al. (2010). Graphene and graphene oxide: synthesis, properties, and applications. *Advanced Materials* 22 (35): 3906–3924.

40 Dikin, D.A., Stankovich, S., Zimney, E.J. et al. (2007). Preparation and characterization of graphene oxide paper. *Nature* 448 (7152): 457–460.

41 Gomez-Navarro, C., Burghard, M., and Kern, K. (2008). Elastic properties of chemically derived single graphene sheets. *Nano Letters* 8 (7): 2045–2049.

42 Chen, H., Müller, M.B., Gilmore, K.J. et al. (2008). Mechanically strong, electrically conductive, and biocompatible graphene paper. *Advanced Materials* 20 (18): 3557–3561.

43 Nair, R.R., Blake, P., Grigorenko, A.N. et al. (2008). Fine structure constant defines visual transparency of graphene. *Science* 320 (5881): 1308.

44 Mak, K.F., Sfeir, M.Y., Wu, Y. et al. (2008). Measurement of the optical conductivity of graphene. *Physical Review Letters* 101 (19): 196405.

45 Ugeda, M.M., Brihuega, I., Hiebel, F. et al. (2012). Electronic and structural characterization of divacancies in irradiated graphene. *Physical Review B* 85 (12): 121402.

46 Nourbakhsh, A., Cantoro, M., Vosch, T. et al. (2010). Bandgap opening in oxygen plasma-treated graphene. *Nanotechnology* 21 (43): 435203.

47 Zhang, C., Fu, L., Liu, N. et al. (2011). Synthesis of nitrogen-doped graphene using embedded carbon and nitrogen sources. *Advanced Materials* 23 (8): 1020–1024.

48 Panchakarla, L.S., Subrahmanyam, K.S., Saha, S.K. et al. (2009). Synthesis, structure, and properties of boron- and nitrogen-doped graphene. *Advanced Materials* 21: 4726–4730.

49 Wang, S., Wang, R., Wang, X. et al. (2012). Nanoscale charge distribution and energy band modification in defect-patterned graphene. *Nanoscale* 4 (8): 2651–2657.

50 Meyer, J.C., Kisielowski, C., Erni, R. et al. (2008). Direct imaging of lattice atoms and topological defects in graphene membranes. *Nano Letters* 8 (11): 3582–3586.

51 Terrones, M., Botello-Méndez, A.R., Campos-Delgado, J. et al. (2010). Graphene and graphite nanoribbons: morphology, properties, synthesis, defects and applications. *Nano Today* 5 (4): 351–372.

52 Ma, J., Alfe, D., Michaelides, A. et al. (2009). Stone-Wales defects in graphene and other planar sp(2)-bonded materials. *Physical Review B* 80 (3): 1132–1136.

53 Yazyev, O.V. and Louie, S.G. (2010). Electronic transport in polycrystalline graphene. *Nature Materials* 9 (10): 806–809.

54 Banhart, F., Kotakoski, J., and Krasheninnikov, A.V. (2011). Structural defects in graphene. *ACS Nano* 5 (1): 26–41.

55 Krasheninnikov, A.V., Lehtinen, P.O., Foster, A.S. et al. (2006). Bending the rules: contrasting vacancy energetics and migration in graphite and carbon nanotubes. *Chemical Physics Letters* 418 (1–3): 132–136.

56 Wintterlin, J. and Bocquet, M.L. (2009). Graphene on metal surfaces. *Surface Science* 603 (10–12): 1841–1852.

57 Lusk, M.T. and Carr, L.D. (2008). Nanoengineering defect structures on graphene. *Physical Review Letters* 100 (17): 175503.

58 Mkhoyan, K.A., Contryman, A.W., Silcox, J. et al. (2009). Atomic and electronic structure of graphene-oxide. *Nano Letters* 9 (3): 1058–1063.

59 Yanjie, G., Litao, S., and Florian, B. (2010). One- and two-dimensional diffusion of metal atoms in graphene. *Small* 4 (5): 587–591.

60 Vinayan, B.P., Nagar, R., Rajalakshmi, N. et al. (2012). Novel platinum-cobalt alloy nanoparticles dispersed on nitrogen-doped graphene as a cathode electrocatalyst for PEMFC applications. *Advanced Materials* 22 (16): 3519–3526.

61 Zhang, X., Yan, F., Zhang, S. et al. (2018). Hollow N-doped carbon polyhedron containing CoNi alloy nanoparticles embedded within few-layer N-doped graphene as high-performance electromagnetic wave absorbing material. *ACS Applied Materials & Interfaces* 10 (29): 24920–24929.

62 Muhich, C.L., Westcott, J.Y., Morris, T.C. et al. (2013). The effect of N and B doping on graphene and the adsorption and migration behavior of Pt atoms. *Journal of Physical Chemistry C* 117 (20): 10523–10535.

63 Bhaviripudi, S., Jia, X., Dresselhaus, M.S. et al. (2010). Role of kinetic factors in chemical vapor deposition synthesis of uniform large area graphene using copper catalyst. *Nano Letters* 10 (10): 4128–4133.

64 Niu, T., Zhou, M., Zhang, J. et al. (2013). Growth intermediates for CVD graphene on Cu(111): carbon clusters and defective graphene. *Journal of the American Chemical Society* 135 (22): 8409–8414.

65 Dutta, S. and Pati, S.K. (2010). Novel properties of graphene nanoribbons: a review. *Journal of Materials Chemistry* 20 (38): 8207.

66 Nakada, K., Fujita, M., Dresselhaus, G. et al. (1996). Edge state in graphene ribbons: Nanometer size effect and edge shape dependence. *Physical Review B* 54 (24): 17954.

67 Son, Y.W., Cohen, M.L., and Louie, S.G. (2006). Half-metallic graphene nanoribbons. *Nature* 444 (7117): 347–349.

68 Xiaolin, L., Xinran, W., Li, Z. et al. (2008). Chemically derived, ultrasmooth graphene nanoribbon semiconductors. *Science* 319 (5867): 1229–1232.

69 Liu, G., Wu, Y., Lin, Y.-M. et al. (2012). Epitaxial graphene nanoribbon array fabrication using BCP-assisted nanolithography. *ACS Nano* 6 (8): 6786–6792.

70 Sokolov, A.N., Yap, F.L., Liu, N. et al. (2013). Direct growth of aligned graphitic nanoribbons from a DNA template by chemical vapour deposition. *Nature Communications* 4: 2402.

71 Fan, X., Peng, Z., Yang, Y. et al. (2015). Atomic H-induced cutting and unzipping of single-walled carbon nanotube carpets with teepee structure and their enhanced supercapacitor performance. 3 (18): 10077–10084.

72 Jinming, C., Pascal, R., Rached, J. et al. (2010). Atomically precise bottom-up fabrication of graphene nanoribbons. *Nature* 466 (7305): 470–473.

73 Qin, K., Kang, J., Li, J. et al. (2016). Continuously hierarchical nanoporous graphene film for flexible solid-state supercapacitors with excellent performance. *Nano Energy* 24: 158–164.

74 Qin, K., Kang, J., Li, J. et al. (2016). Free-standing 3D nanoporous duct-Like and hierarchical nanoporous graphene films for micron-level flexible solid-state asymmetric supercapacitors. *Advanced Energy Materials* 6 (18), 1600755.

75 Zhang, J., Li, C., Peng, Z. et al. (2017). 3D free-standing nitrogen-doped reduced graphene oxide aerogel as anode material for sodium ion batteries with enhanced sodium storage. *Scientific Reports* 7 (1): 4886.

76 Zhu, S., Li, J., Deng, X. et al. (2017). Ultrathin-nanosheet-induced synthesis of 3D transition metal oxides networks for lithium ion battery anodes. *Advanced Functional Materials* 27 (9), 1605017.

77 Qin, J., Zhang, X., Zhao, N. et al. (2015). In situ preparation of interconnected networks constructed by using flexible graphene/Sn sandwich nanosheets for high-performance lithium-ion battery anodes. *Journal of Materials Chemistry A* 3 (46): 23170–23179.

78 Zhu, S., Taberna, P.-L., Zhao, N. et al. (2018). Salt-template synthesis of mesoporous carbon monolith for ionogel-based supercapacitors. *Electrochemistry Communications* 96: 6–10.

79 Zhu, S., Li, J., Li, Q. et al. (2016). Space-confined synthesis of three-dimensional boron/nitrogen-doped carbon nanotubes/carbon nanosheets line-in-wall hybrids and their electrochemical energy storage applications. *Electrochimica Acta* 212: 621–629.

80 Qin, J., Wang, T., Liu, D. et al. (2018). A top-down strategy toward SnSb in-Plane nanoconfined 3D N-doped porous graphene composite microspheres for high performance Na-ion battery anode. *Advanced Materials* 30 (9), 1704670.

81 Wang, Y., Zhang, Y., Liu, J. et al. (2020). Boosting areal energy density of 3D printed all-solid-state flexible microsupercapacitors via tailoring graphene composition. *Energy Storage Materials* 30: 412–419.

82 Jiang, Y., Xu, Z., Huang, T. et al. (2018). Direct 3D printing of ultralight graphene oxide aerogel microlattices. *Advanced Functional Materials* 28 (16), 1707024.

83 Sha, J., Li, Y., Villegas Salvatierra, R. et al. (2017). Three-dimensional printed graphene foams. *ACS Nano* 11 (7): 6860–6867.

84 Wang, H., Wu, L., Xu, L. et al. (2021). Synthetic multiscale graphene aerogel polymer composites with high-conductive performances for hyperthermia equipment. *Advanced Engineering Materials* 23 (7): 2001429.

85 Guo, Y., Ruan, K., Shi, X. et al. (2020). Factors affecting thermal conductivities of the polymers and polymer composites: a review. *Composites Science and Technology* 193: 108134.

86 Fan, X., Nie, W., Tsai, H. et al. (2019). PEDOT:PSS for flexible and stretchable electronics: modifications, strategies, and applications. *Advanced Science* 6 (19): 1900813.

87 Lv, P. (2018). Highly compressible graphene/polypyrrole aerogel for superelastic pseudocapacitors. *Fullerenes, Nanotubes, and Carbon Nanostructures* 26 (1): 23–29.

88 Zhang, Y., Bakenov, Z., Tan, T. et al. (2018). Three-dimensional hierarchical porous structure of PPy/porous-graphene to encapsulate polysulfides for lithium/sulfur batteries. *Nanomaterial* 8 (8): 606.

89 Hu, N., Zhang, L., Yang, C. et al. (2016). Three-dimensional skeleton networks of graphene wrapped polyaniline nanofibers: an excellent structure for high-performance flexible solid-state supercapacitors. *Scitific Reports* 6: 19777.

90 Geng, H., Peng, Y., Qu, L. et al. (2020). Structure design and composition engineering of carbon-based nanomaterials for lithium energy storage. *Advanced Energy Materials* 10 (10).

91 Yu, P., Cao, G., Yi, S. et al. (2018). Binder-free 2D titanium carbide (MXene)/carbon nanotube composites for high-performance lithium-ion capacitors. *Nanoscale* 10 (13): 5906–5913.

92 Meng, T., Li, B., Wang, Q. et al. (2020). Large-scale electric-field confined silicon with optimized charge-transfer kinetics and structural stability for high-rate lithium-ion batteries. *ACS Nano* 14 (6): 7066–7076.

93 Chen, B., Wang, T., Zhao, S. et al. (2021). Efficient reversible conversion between MoS_2 and Mo/Na_2S enabled by graphene-supported single atom catalysts. *Advanced Materials* 33 (12): 2007090.

94 Liu, Y., Zhang, A., Shen, C. et al. (2017). Red phosphorus nanodots on reduced graphene oxide as a flexible and ultra-fast anode for sodium-ion batteries. *ACS Nano* 11 (6): 5530–5537.

95 Lv, Y., Fang, Y., Wu, Z. et al. (2015). In-situ confined growth of monodisperse pt nanoparticle@graphene nanobox composites as electrocatalytic nanoreactors. *Small* 11 (8): 1003–1010.

96 Perera, S.D., Mariano, R.G., Vu, K. et al. (2012). Hydrothermal synthesis of graphene-TiO_2 nanotube composites with enhanced photocatalytic activity. *ACS Catalysis* 2 (6): 949–956.

97 Perera, S.D., Mariano, R.G., Vu, K. et al. (2016). Facile hydrothermal synthesis of $SnCoS_4$/graphene composites with excellent electrochemical performance for reversible lithium ion storage. *Journal of Materials Chemistry A* 4 (34): 13194–13202.

98 Kuang, D.A., Liye, X.U., Lei, L. et al. (2013). Graphene-nickel composites. *Applied Surface Science* 273 (6): 484–490.

99 Gao, M., Cui, X., Wang, R. et al. (2015). Graphene-wrapped mesoporous $MnCO_3$ single crystals synthesized by a dynamic floating electrodeposition method for high performance lithium-ion storage. *Journal of Materials Chemistry A* 3 (27): 14126–14133.

100 Li, S.-M., Wang, Y.S., Yang, S.Y. et al. (2013). Electrochemical deposition of nanostructured manganese oxide on hierarchically porous graphene-carbon

nanotube structure for ultrahigh-performance electrochemical capacitors. *Journal of Power Sources* 225: 347–355.

101 Giampiccolo, A., Tobaldi, D.M., Leonardi, S.G. et al. (2019). Sol-gel graphene/TiO_2 nanoparticles for the photocatalytic-assisted sensing and abatement of NO_2. *Applied Catalysis B: Environmental* 243: 183–194.

102 Li, W., Wang, F., Liu, Y. et al. (2015). General strategy to synthesize uniform mesoporous TiO_2/graphene/mesoporous TiO_2 sandwich-like nanosheets for highly reversible lithium storage. *Nano Letters* 15 (3): 2186–2193.

103 Zhang, F., Yi, F., Meng, T. et al. (2019). In situ supramolecular self-assembly assisted synthesis of $Li_4T_{i5}O_{12}$-carbon-reduced graphene oxide microspheres for lithium-ion batteries. *ACS Sustainable Chemistry & Engineering* 7 (1): 916–924.

104 Wu, H., Tang, Q., Fan, H. et al. (2017). Dual-confined and hierarchical-porous graphene/C/SiO_2 hollow microspheres through spray drying approach for lithium-sulfur batteries. *Electrochimica Acta* 255: 179–186.

105 Sun, Z., Guo, Y., Li, B. et al. (2019). ZnO/carbon nanotube/reduced graphene oxide composite film as an effective interlayer for lithium/sulfur batteries. *Solid State Sciences* 95: 105924.

106 Chen, S., Bao, P., Xiao, L. et al. (2013). Large-scale and low cost synthesis of graphene as high capacity anode materials for lithium-ion batteries. *Carbon* 64 (11): 158–169.

107 Zhao, B., Liu, P., Jiang, Y. et al. (2012). Supercapacitor performances of thermally reduced graphene oxide. *Journal of Power Sources* 198: 423–427.

108 Lewis, G.D.A., Yi, Z., Schlenker, C.W. et al. (2010). Continuous, highly flexible, and transparent graphene films by chemical vapor deposition for organic photovoltaics. *ACS Nano* 4 (5): 2865–2873.

109 Nechiyil, D., Vinayan, B.P., and Ramaprabhu, S. (2017). Tri-iodide reduction activity of ultra-small size PtFe nanoparticles supported nitrogen-doped graphene as counter electrode for dye-sensitized solar cell. *Journal of Colloid and Interface Science* 488: 309–316.

110 Hwang, J., Yoon, T., and Jin, S.H. (2013). Enhanced mechanical properties of graphene/copper nanocomposites using a molecular-level mixing process. *Advanced Materials* 25 (46): 6724–6729.

111 Li, W., Yang, X., He, C. et al. (2019). Compressive responses and strengthening mechanisms of aluminum composite foams reinforced by graphene nanosheets. *Carbon* 153: 396–406.